PII: S0955-2219(98)00169-1

0955-2219/98/$—see front matter

The Perovskite Oxide System $Pr_{1-x}Sr_xCo_{1-y}Mn_yO_{3-\delta}$: Crystal Structure and Thermal Expansion

G. Ch. Kostogloudis, P. Fertis and Ch. Ftikos*

Laboratory of Inorganic Materials Technology, Department of Chemical Engineering, National Technical University of Athens, 9 Heroon Polytechniou Str., Zografou Campus, GR-157 80 Athens, Greece

(Received 7 January 1998; accepted 29 June 1998)

Abstract

The crystal structure and thermal expansion of the perovskite oxides in the system $Pr_{1-x}Sr_xCo_{1-y}Mn_yO_{3-\delta}$ ($x = 0{\cdot}3$, $0{\cdot}5$, $0 \le y \le 1$) were studied in air, by X-ray powder diffraction and dilatometry, respectively. All compositions have an orthorhombic $GdFeO_3$-type structure (Pbnm space group). The lattice parameters were determined at room temperature. The pseudo-cubic lattice constant decreases on increasing Co content. The thermal expansion coefficient increases as the Co content of the oxides increases for both series with 30 and 50 mol% Sr. Among the Co-containing compositions, those with 20 mol% Co exhibit thermal expansion compatibility with $Ce_{0.9}Gd_{0.1}O_{1.95}$ electrolyte in the whole examined temperature range (room temperature to 800°C). They can be considered, therefore, as candidate cathode materials for intermediate temperature solid oxide fuel cells.

1 Introduction

$RE_{1-x}Sr_xBO_3$ (RE = rare earth, B = transition metal) perovskite oxides have been extensively investigated in recent years, due to their potential utilization as cathodes in solid oxide fuel cells (SOFC).[1] For high temperature operation (900–1000°C) there is a general agreement on the use of $La_{1-x}Sr_xMnO_{3\pm\delta}$ ($0{\cdot}16 \le x \le 0{\cdot}3$) in contact with yttria stabilized zirconia (YSZ) solid electrolyte.[1–4] For intermediate temperatures (500–700°C), however, Co-containing compositions have been proposed, that have better oxide-ion conductivity and electrocatalytic behavior than pure manganites.[3,5,6] As for the electrolyte, $Ce_{0.9}Gd_{0.1}O_{1.95}$ (CGO) is considered more appropriate for intermediate temperature operation, since it possesses higher conductivity than YSZ, and its thermal expansion coefficient (TEC) [around $12{\cdot}5\times10^{-6}$ cm (cm °C)$^{-1}$] is compatible with that of ferritic stainless steel interconnect.[3]

An important criterion, that the cathode material should meet, is thermal expansion compatibility with the electrolyte. Previous studies on the perovskite oxide systems $Pr_{1-x}Sr_xMnO_{3\pm\delta}$[7] and $Pr_{1-x}Sr_xCoO_{3-\delta}$[8] have shown that the TEC of the manganites is nearly equal or lower than that of CGO, while the TEC of the cobaltites is considerably higher [above 18×10^{-6} cm (cm °C)$^{-1}$]. Moreover, the TEC increases with increasing Sr content in $Pr_{1-x}Sr_xMnO_{3\pm\delta}$, and decreases in $Pr_{1-x}Sr_xCoO_{3-\delta}$. In the present study the mixed system $Pr_{1-x}Sr_xCo_{1-y}Mn_yO_{3-\delta}$ ($x = 0{\cdot}3$, $0{\cdot}5$, $0 \le y \le 1$) was examined. The effect of the B-site composition, as well as of the Sr doping level, on the structural and thermal expansion properties of these oxides was investigated. Electrical conductivity measurements were also performed for the $Pr_{1-x}Sr_xCo_{1-y}Mn_yO_{3-\delta}$ system, and they are presented and discussed in a separate paper.[9]

2 Experimental

The $Pr_{1-x}Sr_xCo_{1-y}Mn_yO_{3-\delta}$ powders were prepared by the citrate synthesis and pyrolysis method.[10] The reagents Pr_6O_{11}, $Sr(NO_3)_2$, $(CH_3COO)_2Co{\cdot}4H_2O$ and $(CH_3COO)_2Mn(4H_2O)$, all of high purity, were separately dissolved in distilled water or nitric acid, in the correct molar proportions.

*To whom correspondence should be addressed.

The individual solutions were mixed together and an aqueous solution of citric acid was added. The final solution was heated over a burner flame, and after vaporization and subsequent pyrolysis, a powder was obtained. The powder was calcined at 1100°C for 15 h, wet milled with acetone using zirconia balls, dried, and compacted in the shape of cylindrical rods (approximate dimensions: 50 mm length and 6 mm diameter) by cold isostatic pressing at 300 MPa. The compacts were sintered in air at 1300°C for 15 h, with a heating and cooling rate of 1°C min^{-1}. The bulk density of the sintered rods was measured by the Archimedes method[7] using distilled water as the liquid medium. Selected sintered samples were examined by optical microscopy on polished surfaces.

The crystal structure at room temperature was determined on oxide powders by X–ray powder diffraction (XPD). The powders were fired at 1300°C and then slowly cooled to room temperature. The measurements were performed in the range 10–80° 2θ on a Siemens D5000 diffractometer, using CuKα radiation, and operated at 40 kV and 30 mA. The unit cell parameters were determined from the XPD data using the LSUCR (Least Squares Unit Cell Refinement) computer program.

The thermal expansion measurements were performed in air on the sintered cylindrical rods using a quartz dilatometer. The data were collected upon cooling from 800 to 100°C, at a cooling rate of 5°C min^{-1}.

3 Results and Discussion

3.1 Crystal structure

The XPD patterns of the oxides in the system $Pr_{1-x}Sr_xCo_{1-y}Mn_yO_{3-\delta}$ are shown in Figs 1 and 2, for $x=0{\cdot}3$ and $0{\cdot}5$, respectively. As can be seen in Fig. 1, the pattern of the manganite end member ($y=1$) of the series with 30 mol% Sr is symmetric, while on Co substitution a peak splitting is established, whose magnitude gradually increases. The opposite trend can be observed for the series of oxides with 50 mol% Sr (Fig. 2). In this case, the manganite end member exhibits a peek splitting, which is gradually reduced as the Co content increases.

For all compositions, the patterns were indexed in the orthorhombic $GdFeO_3$-type[11] structure (Pbnm space group). This type of structure is common for rare earth perovskite-type oxides.[12] Each unit cell consists of four ABO_3 units, and has the approximate dimensions $\sqrt{2}a_p \times \sqrt{2}a_p \times 2a_p$, where a_p is the lattice parameter of the ideal cubic unit cell. The determined lattice parameters of the orthorhombic cell are shown in Table 1. They are also drawn in Figs 3 and 4, for the series with 30 and 50 mol% Sr, respectively. As can be seen, the substitution of Co for Mn causes an increase of the deviation among the parameters a, b, $c/\sqrt{2}$ for the series with $x=0{\cdot}3$ (Fig. 3). On the other hand, a decrease of the deviation among the parameters can be observed on Co substitution for the series with $x=0{\cdot}5$ (Fig. 4). The orthorhombic deformation, D, defined as:[13]

$$D = \frac{1}{3}\sum_{i=1}^{3} \left| \frac{a_i - \bar{a}}{\bar{a}} \right| \times 100 \qquad (1)$$

where $a_1 = a$, $a_2 = b$, $a_3 = c/\sqrt{2}$, and $\bar{a} = \left(abc/\sqrt{2}\right)^{1/3}$, is also shown in Figs 3 and 4. D quantitatively expresses the macroscopic distortion relative to the ideal perovskite structure. For $x=0{\cdot}3$, D increases on increasing Co content, while the opposite applies for $x=0{\cdot}5$. These results are consistent with the observations concerning the splitting of the XPD peaks, described above.

The relation among the lattice parameters, a, b and $c/\sqrt{2}$, can provide a measure of the distortion of the unit cell. This relation is included in Table 1. Generally, two types of orthorhombic structures are distinguished. The O-type structure, which is characterized by the relationship $a \leq c/\sqrt{2} \leq b$, exists when the lattice deformation is relatively small, while the O′-type structure, with $c/\sqrt{2} \leq a \leq b$, exists in the case of enhanced lattice deformation. The structure of $Pr_{0{\cdot}7}Sr_{0{\cdot}3}Co_{1-y}Mn_yO_{3-\delta}$ is O′-type for $0 \leq y \leq 0{\cdot}6$ and O-type for $y=0{\cdot}8$ and 1. The structure of $Pr_{0{\cdot}5}Sr_{0{\cdot}5}Co_{1-y}Mn_yO_{3-\delta}$, on the other hand, is O-type for $y=0$, $0{\cdot}2$ and $0{\cdot}4$, and O′-type for $y=0{\cdot}6$, $0{\cdot}8$ and 1.

The pseudo-cubic lattice constant a', defined as:

$$a' = (V/z)^{1/3} \qquad (2)$$

where $z=4$ for the $Pr_{1-x}Sr_xCo_{1-y}Mn_yO_{3-\delta}$ oxides of this study, is drawn in Fig. 5. As can be seen, a' decreases on increasing Co content for both series of oxides with $x=0{\cdot}3$ and $0{\cdot}5$. However, a more steep decrease is observed in the case of the series containing 30 mol% Sr. The change in the size of a' depends on factors such us the difference in the ionic radius of the dopant cation (Sr^{2+}) in relation to the host cation (Pr^{3+}), as well as the ionic radii difference between the transition metals at the B-site. The introduction of Sr^{2+} cation on a Pr^{3+} lattice position, at high oxygen partial pressures and low temperatures, is electronically compensated by the oxidation of the transition metal to the tetravalent state, according to the defect reaction:

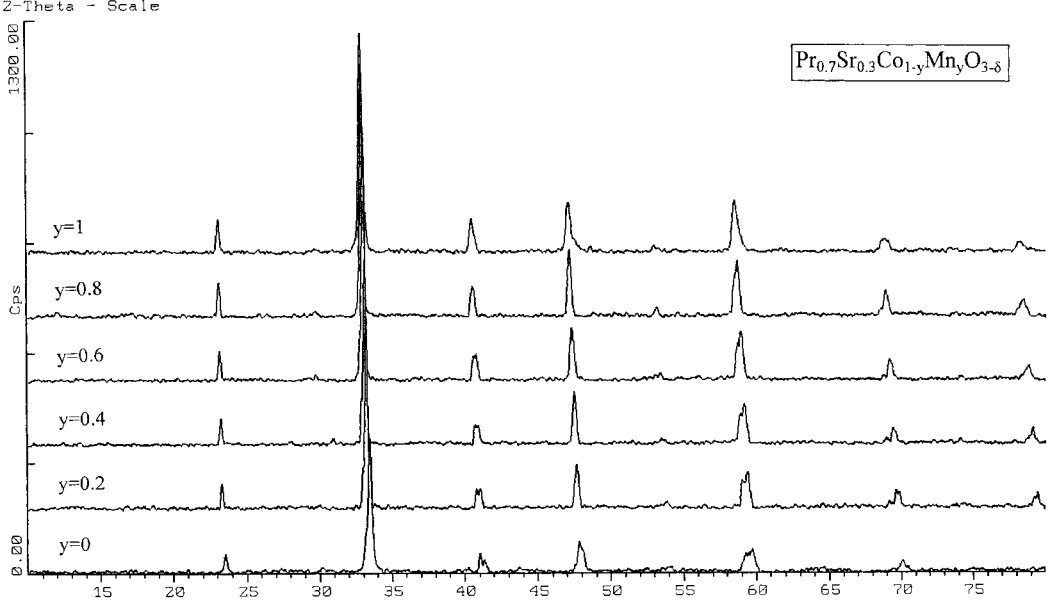

Fig. 1. X-ray powder diffraction patterns of $Pr_{0.7}Sr_{0.3}Co_{1-y}Mn_yO_{3-\delta}$.

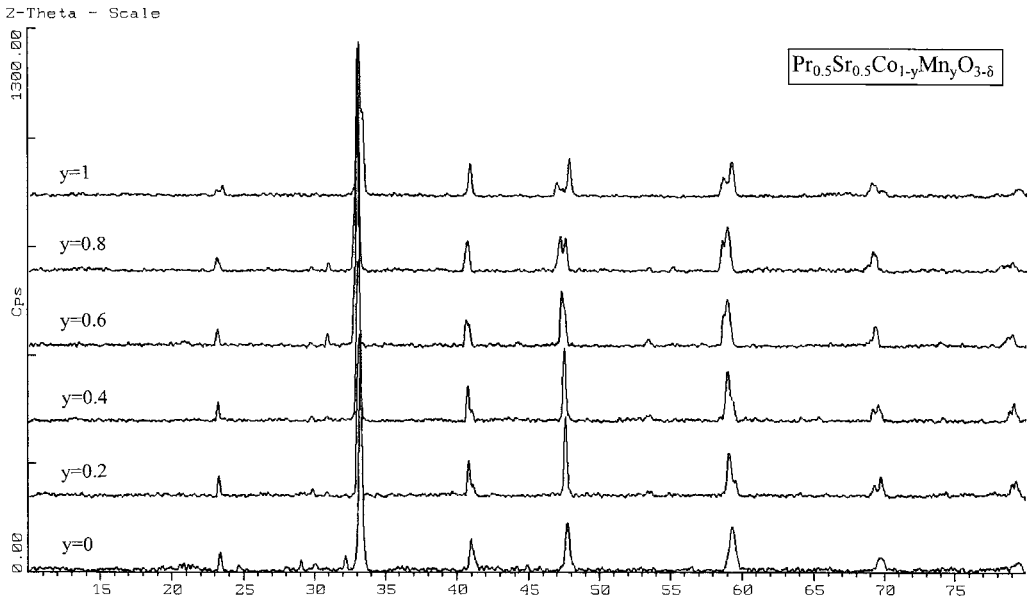

Fig. 2. X-ray powder diffraction patterns of $Pr_{0.5}Sr_{0.5}Co_{1-y}Mn_yO_{3-\delta}$.

Table 1. Phase symmetry, lattice parameters, unit cell volume, orthorhombic deformation D (%), and type of orthorhombic structure of the system $Pr_{1-x}Sr_xCo_{1-y}Mn_yO_{3-\delta}$

y *(mol)*	*Phase symmetry*	a *(Å)*	b *(Å)*	c *(Å)*	*Volume (Å^3)*	$c/\sqrt{2}$ *(Å)*	a,b,c/$\sqrt{2}$ *relation*	*Orthorhombic deformation D (%)*	*Type of orthorhombic structure*
$Pr_{0.7}Sr_{0.3}Co_{1-y}Mn_yO_{3-\delta}$									
0	Orthorhombic	5·3502	5·3982	7·5657	218·51	5·3498	$c/\sqrt{2} < a < b$	0·399	O′-type
0·2	Orthorhombic	5·3911	5·3969	7·5740	220·37	5·3556	$c/\sqrt{2} < a < b$	0·317	O′-type
0·4	Orthorhombic	5·4080	5·4181	7·6252	223·43	5·3918	$c/\sqrt{2} < a < b$	0·175	O′-type
0·6	Orthorhombic	5·4245	5·4414	7·6687	226·36	5·4226	$c/\sqrt{2} < a < b$	0·146	O′-type
0·8	Orthorhombic	5·4460	5·4552	7·7066	228·96	5·4494	$a < c/\sqrt{2} < b$	0·061	O-type
1	Orthorhombic	5·4598	5·4681	7·7416	231·12	5·4741	$a < b < c/\sqrt{2}$	0·092	O-type
$Pr_{0.5}Sr_{0.5}Co_{1-y}Mn_yO_{3-\delta}$									
0	Orthorhombic	5·3818	5·3889	7·6189	220·96	5·3874	$a < c/\sqrt{2} < b$	0·052	O-type
0·2	Orthorhombic	5·3919	5·4147	7·6613	223·68	5·4174	$a < b < c/\sqrt{2}$	0·198	O-type
0·4	Orthorhombic	5·4062	5·4235	7·6779	225·12	5·4291	$a < b < c/\sqrt{2}$	0·165	O-type
0·6	Orthorhombic	5·4196	5·4523	7·6572	226·26	5·4145	$c/\sqrt{2} < a < b$	0·289	O′-type
0·8	Orthorhombic	5·4371	5·4651	7·6510	227·34	5·4101	$c/\sqrt{2} < a < b$	0·339	O′-type
1	Orthorhombic	5·4309	5·5165	7·5937	227·50	5·3696	$c/\sqrt{2} < a < b$	0·948	O′-type

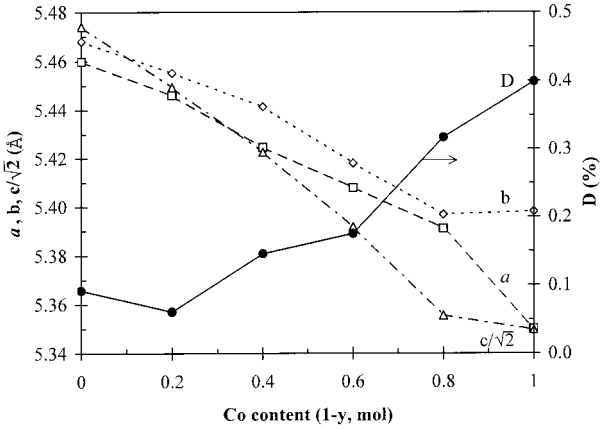

Fig. 3. Lattice parameters (a,b,$c/\sqrt{2}$) and orthorhombic deformation (D, %) of $Pr_{0.7}Sr_{0.3}Co_{1-y}Mn_yO_{3-\delta}$ as a function of Co content ($1-y$, mol).

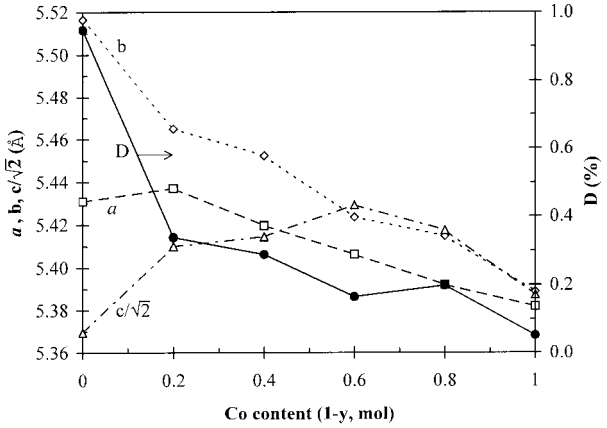

Fig. 4. Lattice parameters (a,b,$c/\sqrt{2}$) and orthorhombic deformation (D, %) of $Pr_{0.5}Sr_{0.5}Co_{1-y}Mn_yO_{3-\delta}$ as a function of Co content ($1-y$, mol).

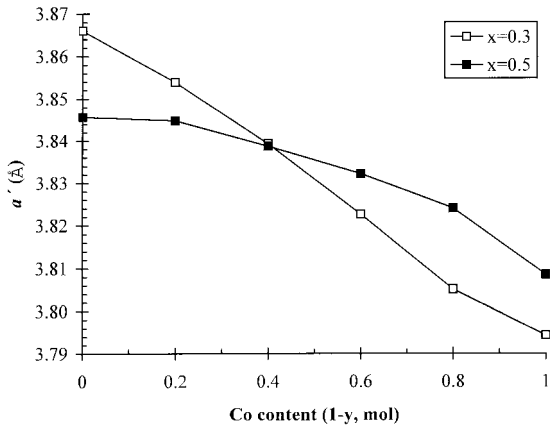

Fig. 5. Pseudo-cubic lattice constant (a') of $Pr_{1-x}Sr_xCo_{1-y}Mn_yO_{3-\delta}$ as a function of Co content ($1-y$, mol).

$$PrBO_3 \xrightarrow{SrO} Pr^x_{1-x}Sr'_xB^x_{1-x}B^{\bullet}_xO_3 \qquad (3)$$

where Pr^x and B^x are Pr^{3+} and B^{3+} cations, respectively, on regular sites, Sr' is a Sr^{2+} cation on a Pr^{3+} lattice position and $B^{\bullet}$ is a B^{4+} cation on a B^{3+} position in the perovskite lattice. In Table 2,

Table 2. Ionic radii of several cations, and their coordination number (CN) in the perovskite lattice[14]

Cation	*Ionic radius (Å)*
Pr^{3+} (CN = 12)	1·30
Sr^{2+} (CN = 12)	1·44
Co^{3+} (CN = 6)	0·545
Co^{4+} (CN = 6)	0·53
Mn^{3+} (CN = 6)	0·645
Mn^{4+} (CN = 6)	0·530

the ionic radii of the cations involved in this study are shown, according to Shannon.[14] If we consider a fixed composition at the A-site, inspection of the transition metal ionic radii (Table 2) reveals that while the tetravalent Co and Mn ions have equal sizes, the Co^{3+} cation is smaller than the Mn^{3+} cation. Therefore, irrespective of the Sr content of the perovskite (30 or 50 mol%), the cobaltite end member is expected to have a smaller lattice constant than the manganite end member. Moreover, since a higher concentration of trivalent cations exists in the oxides with $x = 0{\cdot}3$ than $x = 0{\cdot}5$, the magnitude of the decrease of a' is expected to be higher in the former case, because this involves the substitution of a higher Mn^{3+} cation concentration by Co^{3+}.

3.2 Density

The sintering temperature, the measured sintered density (d), the theoretical density (d_{th}), and the d/d_{th} are shown in Table 3. The theoretical density (or X-ray density) was calculated (in g cm^{-3}) by the equation:[15]

$$d_{th} = z\frac{M}{V \times 0{\cdot}6023} \qquad (4)$$

where M (in atomic-weight units) is the mass of a ABO_3 unit, z is the number of ABO_3 units in one unit cell of the crystal ($z = 4$), and V (in $Å^3$) is the volume of the crystalline unit cell as determined by X-ray diffraction ($V = abc$ for the orthorhombic unit cell). All samples had densities above 94·5% of the theoretical values. From optical microscopy examination on selected compositions, no open porosity could be observed.

3.3 Thermal expansion

The thermal expansion curves for the compositions in the system $Pr_{1-x}Sr_xCo_{1-y}Mn_yO_{3-\delta}$ are shown in Figs 6 and 7 for $x = 0{\cdot}3$ and 0·5, respectively. All curves are almost linear, but in most cases the slope increases at high temperatures. This can be attributed to the loss of lattice oxygen and the formation of oxygen vacancies ($V^{\bullet\bullet}_O$), according to the defect reaction:

Table 3. Sintering temperature, measured sintered density (d), theoretical XRD density (d_{th}), and d/d_{th} (%) of $Pr_{1-x}Sr_xCo_{1-y}Mn_yO_{3-\delta}$

y (mol)	*Sintering temperature (°C)*	*Sintered density* d *(g cm^{-3})*	*XRD density* d_{th} *(g cm^3)*	d/d_{th} *(%)*
$Pr_{0.7}Sr_{0.3}Co_{1-y}Mn_yO_{3-\delta}$				
0	1300	6·77	7·05	96·0
0·2	1300	6·84	6·96	98·3
0·4	1300	6·74	6·84	98·5
0·6	1300	6·54	6·73	97·2
0·8	1300	6·49	6·63	97·9
1	1300	6·37	6·55	97·3
$Pr_{0.5}Sr_{0.5}Co_{1-y}Mn_yO_{3-\delta}$				
0	1300	6·37	6·65	95·8
0·2	1300	6·36	6·54	97·2
0·4	1300	6·36	6·48	98·1
0·6	1300	6·32	6·42	98·4
0·8	1300	6·04	6·37	94·8
1	1300	5·99	6·34	94·5

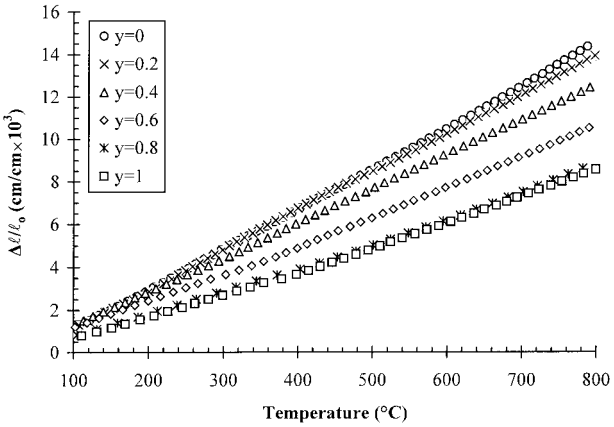

Fig. 6. Linear thermal expansion curves for $Pr_{0.7}Sr_{0.3}Co_{1-y}Mn_yO_{3-\delta}$ in air.

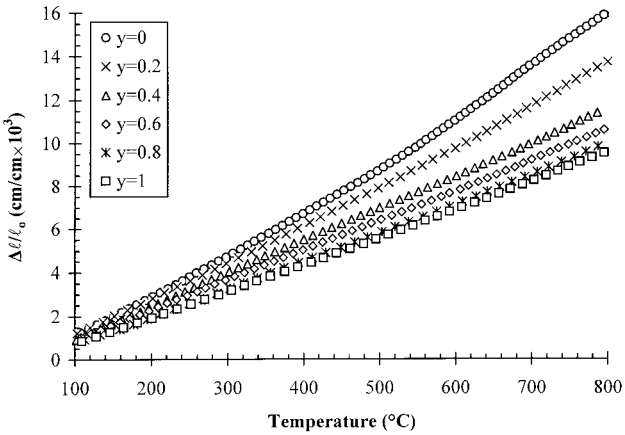

Fig. 7. Linear thermal expansion curves for $Pr_{0.5}Sr_{0.5}Co_{1-y}Mn_yO_{3-\delta}$ in air.

$$Pr^{x}_{1-x}Sr'_{x}B^{x}_{1-x}B^{\bullet}_{x}O_3 = Pr^{x}_{1-x}Sr'_{x}B^{x}_{1-x+2\delta}B^{\bullet}_{x-2\delta}O_{3-\delta}[\delta\, V^{\bullet\bullet}_{O}] + \frac{\delta}{2}O_2 \quad (5)$$

where B = Mn or Co. As the temperature increases, and more oxygen vacancies are formed, eqn (5) shifts to the right, and as a result the reduction $B^{4+} \rightarrow B^{3+}$ takes place. Considering the ionic radii difference between the two oxidation states of the transition metals (Table 2), it can be inferred that a lattice expansion is expected to occur when the concentration of B^{3+} ions is increased. In addition, the reduction of the B^{4+} cations causes a decrease in the B–O bond strength according to Pauling's second rule,[16] and hence the size of BO_6 octahedra increases, thus enhancing the lattice expansion.

The linear thermal expansion coefficients (TEC) of the oxides were calculated from the slopes of the curves of Figs 6 and 7, and they are shown in Table 4 for the given temperature ranges. They are also drawn in Fig. 8 as a function of Co content, for the series with $x = 0{\cdot}3$ and 0·5 and for 500 and 700°C (the operating temperatures of interest for the intermediate temperature SOFC). The TEC is higher at elevated temperatures, as a result of the increase in the slope of the thermal expansion curves. Figure 8 reveals that the TEC increases on increasing Co content for both series of oxides and for both 500 and 700°C.

According to the theory of thermal expansion developed by Ruffa,[17] the TEC is inversely proportional to the nearest neighbor distance r_n, which can be approximated to the metal-oxide ion bond length. Since in this study the exact interatomic distances were not determined, we can approximate r_n to half the pseudo-cubic lattice constant ($a'/2$). Therefore, the observed increase of the TEC with increasing Co content, can be explained considering the concurrent decrease of a' (Fig. 5).

A more detailed inspection of Fig. 8 (TEC) in comparison with Fig. 5 (a') leads to the following conclusions: At 700°C and for Co content in the range $0 \leq 1-y \leq 0{\cdot}4$ the TEC is greater for the $x = 0{\cdot}5$ series, as a result of their smaller a' values.

Table 4. Linear thermal expansion coefficients (TEC) of $Pr_{1-x}Sr_xCo_{1-y}Mn_yO_{3-\delta}$

y *(mol)*	*Temperature range (°C)*	*Linear TEC [cm(cm°C)$^{-1}$×10^6]*
$Pr_{0.7}Sr_{0.3}Co_{1-y}Mn_yO_{3-\delta}$		
0	100–700	18·9
	700–800	20·7
0·2	100–800	18·3
0·4	100–800	16·2
0·6	100–500	12·6
	500–800	14·5
0·8	100–550	10·6
	550–800	13·2
1	100–500	10·5
	500–800	12·5
$Pr_{0.5}Sr_{0.5}Co_{1-y}Mn_yO_{3-\delta}$		
0	100–500	19·1
	500–800	24·6
0·2	100–550	17·0
	550–800	19·8
0·4	100–800	15·1
0·6	100–600	13·6
	600–800	14·7
0·8	100–600	12·8
	600–800	14·4
1	100–600	12·2
	600–800	13·6

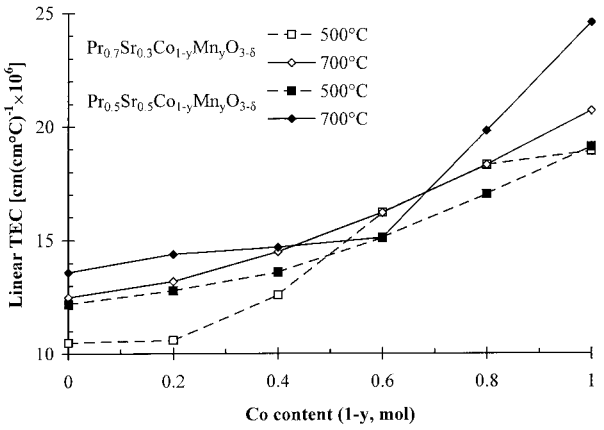

Fig. 8. Linear thermal expansion coefficient (TEC) values of $Pr_{1-x}Sr_xCo_{1-y}Mn_yO_{3-\delta}$ at 500 and 700°C as a function of Co content ($1-y$, mol) in air.

For $1-y=0{\cdot}6$ the TEC of $x=0{\cdot}5$ becomes lower, since its a' becomes larger. For even higher values of Co content ($1-y\geq0{\cdot}8$) the TEC of $x=0{\cdot}5$ is greater, even though its a' value is still larger. This change in the relationship between TEC and a' for Co-rich compositions is attributed to the formation of oxygen vacancies at high temperatures (>600°C), that results in enhanced lattice expansion. The rate of oxygen vacancy formation for cobaltites has been shown to be greater for $x=0{\cdot}5$ than for $x=0{\cdot}3$.[8,18,19] The relationship between TEC and a' (TEC increases when a' decreases) is maintained for 500°C and for Co content in the range $0\leq1-y\leq0{\cdot}8$, but it does not hold in the case of the cobaltite end members. This is again due to the formation of oxygen vacancies in the case of the $x=0{\cdot}5$ compound, even from room temperature.[8]

Among the Co-containing perovskite oxides of this study, those with 20 and 40 mol% Co possess acceptable TEC values for SOFC operation at 500°C, if CGO electrolyte is used. At 700°C, the compositions with 20 mol% Co exhibit good thermal expansion compatibility with CGO electrolyte. Between the two Sr doping levels of 30 and 50 mol%, the one with 30 mol% Sr would probably be more appropriate from the chemical compatibility point of view, since for high x values the chemical stability of the cathode material in contact with the electrolyte is usually reduced.[20,21] This issue, though, is still to be investigated.

4 Conclusions

The perovskite oxides in the system $Pr_{1-x}Sr_xCo_{1-y}Mn_yO_{3-\delta}$ ($x=0{\cdot}3$, $0{\cdot}5$, $0\leq y\leq1$) have an orthorhombic $GdFeO_3$-type structure. The orthorhombic deformation increases on increasing Co content for the series with 30 mol% Sr, while it decreases for the series with 50 mol% Sr. The pseudo-cubic lattice constant decreases with increasing Co content for both series of oxides, as a result of the smaller ionic radius of Co^{3+} compared to that of Mn^{3+}. The greater magnitude of the lattice constant decrease for the $x=0{\cdot}3$ series, in comparison with the $x=0{\cdot}5$ series, arises from the fact that a higher Co^{3+} concentration is substituted for Mn^{3+} in the former case.

The linear thermal coefficient (TEC) is generally greater at high temperatures due to the loss of lattice oxygen and the formation of oxygen vacancies. The TEC increases on increasing Co content for both series of oxides (with 30 and 50 mol% Sr) and for both low and high temperature intervals. Among the Co-containing compositions, those with 20 mol% Co exhibit good thermal expansion compatibility with CGO electrolyte up to 800°C.

References

1. Minh, N. Q., Ceramic fuel cells. *J. Am. Ceram. Soc.*, 1993, **76**, 563–588.
2. Hammou, A., Solid oxide fuel cell. In *Advances in Electrochemical Science and Engineering*, Vol. 2, ed. H. Gerischer and C. W. Tobias, VCH, Weinheim, Germany, 1992, pp. 87–139.
3. Steel, B. C. H., Materials for high-temperature fuel cells. *Phil. Trans. R. Soc. Lond. A*, 1996, **354**, 1695–1710.
4. Wilkenhöhner, R., Malléner, W., Buchkremer, H. P., Hauber, Th. and Stimming, U. In Proceedings of the 2nd European SOFC Forum, Oslo, 1996.
5. Steele, B. C. H., Carter, S., Kajda, J., Kontoulis, I. and Kilner, J. A., Optimisation of fuel cell components using

$^{18}O/^{16}O$ exchange and dynamic SIMS techinques. In *Proceedings of the 2nd International Symposium on Solid Oxide Fuel Cells*, ed. F. Grosz, P. Zegers, S. C. Singhal and O. Yamamoto. The Electrochemical Society, Pennington, NJ, 1991, pp. 517–525.
6. Steele, B. C. H., Oxygen transport and exchange in oxide ceramics. *J. Power Sources*, 1994, **49**, 1.
7. Kostogloudis, G. Ch., Vasilakos, N. and Ftikos, Ch., Preparation and characterization of $Pr_{1-x}Sr_xMnO_{3\pm\delta}$ ($x=0$, 0·15, 0·3, 0·4, 0·5) as a potential SOFC cathode material operating at intermediate temperatures (500–700°C). *Journal of the European Ceramic Society*, 1997, **17**, 1513–1521.
8. Kostogloudis, G. Ch., Vasilakos, N. and Ftikos, Ch., Crystal structure, thermal and electrical properties of $Pr_{1-x}Sr_xCoO_{3-\delta}$ ($x=0$, 0·15, 0·3, 0·4, 0·5) perovskite oxides. *Solid State Ionics*, 1998, **106**, 207–218.
9. Kostogloudis, G. Ch., Fertis, P. and Ftikos Ch., Electronic conductivity in the $Pr_{1-x}Sr_xCo_{1-y}Mn_yO_{3-\delta}$ system. *Solid State Ionics*, in press.
10. Blank, D. H. A., Kruidhof, H. and Flokstra, J., Preparation of $YBa_2Cu_3O_{7-\delta}$ by citrate synthesis and pyrolysis. *J. Phys. D*, 1988, **21**, 226–227.
11. Geller, S., *J. Chem. Phys.*, 1956, **24**, 1236.
12. Demazeau, G., Pouchard, M. and Hagenmuller, P., Sur de nouveaux composés exygénés du cobalt +III dérivés de la perovskite. *J. Solid State Chem.*, 1974, **9**, 202–209.
13. Knízek, K., Jirak, Z., Pollert, E. and Zounova, F., Structure and magnetic properties of $Pr_{1-x}Sr_xMnO_3$ perovskites. *J. Solid State Chem.*, 1992, **100**, 292–300.
14. Shannon, R. D., Revised effective ionic radii and systematic studies of interatomic distance in halides and chalcogenides. *Acta Crystallogr.*, 1976, **A32**, 751–767.
15. Raman, S. and Katz, J. L., X-ray methods of determining crystal structures. In *Handbook of X-Rays*, ed. E. F. Kaelble. McGraw–Hill, New York, 1967, pp. 29.1–29.2.
16. Pauling, L., *The Nature of the Chemical Bond*, 3rd edn. Cornell University Press, Ithaca, NY, 1960, pp. 547–559.
17. Ruffa, A. R., Thermal expansion in insulating materials. *J. Mater. Sci.*, 1980, **15**, 2258–2267.
18. Jonker, G. H. and van Santen, J. H., *Physica*, 1953, **19**, 120.
19. Petrov, A. N., Kononchuk, O. F., Andreev, A. V., Cherepanov, V. A. and Kofstad, P., Crystal structure, electrical and magnetic properties of $La_{1-x}Sr_xCoO_{3-y}$. *Solid State Ionics*, 1995, **80**, 189–199.
20. Yokokawa, H., Sakai, N., Kawada, T. and Dokiya, M., Thermodynamic analysis on interface between perovskite electrode and YSZ electrolyte. *Solid State Ionics*, 1990, **40/41**, 398–401.
21. Kindermann, L. and Hilpert, K. Chemical compatibility of $LaFeO_3$ based perovskites with yttria stabilized zirconia. In *Proceedings of the 5th International Symposium on Solid Oxide Fuel Cells*, Vol. 97–40, ed. U. Stimming, S. C. Singhal, H. Tagawa and W. Lehnert. The Electrochemical Society, Pennington, NJ, 1997, pp. 773–782.